Applied Catalysis A: General 528 (2016) 67–73

Contents lists available at ScienceDirect

Applied Catalysis A: General

journal homepage: www.elsevier.com/locate/apcata

In-situ X-ray absorption study of ceria-supported Pd-Cu nanoparticles for oxygen-enhanced water gas shift

Junichiro Kugai[a,**], Jeffrey T. Miller[b], Elise B. Fox[c], Chunshan Song[a,*]

[a] Clean Fuels and Catalysis Program, EMS Energy Institute, and Department of Energy and Mineral Engineering, The Pennsylvania State University, 209 Academic Projects Building, University Park, PA 16802, USA
[b] School of Chemical Engineering, Purdue University, 480 Stadium Mall Drive, West Lafayette, IN 47907-2100, USA
[c] Materials Science & Technology, Savannah River National Laboratory, Aiken, SC 29808, USA

ARTICLE INFO

Article history:
Received 4 April 2016
Received in revised form 8 September 2016
Accepted 18 September 2016
Available online 19 September 2016

Keywords:
Extended X-ray absorption fine structure (EXAFS)
CeO_2-supported Pd-Cu
Bimetallic catalyst
Pd-Cu alloy
Oxygen-enhanced water gas shift (OWGS)

ABSTRACT

The detailed structures of bimetallic Pd-Cu on various CeO_2 and Al_2O_3 supports were investigated by X-ray absorption technique in-situ in hydrogen and WGS conditions. No indication of the neighboring Pd atoms in both Pd-*K* edge and Cu-*K* edge EXAFS fittings showed that Pd is highly dispersed in the lattice of metallic Cu. The Cu-Cu bond distance was markedly shortened by alloying with Pd and correlated to decrease of coordination number, which reflects particle size. A higher coordination number for Pd-Cu than that for Cu-Cu on Al_2O_3 support suggested that Pd is in the interior of the nanoparticles on Al_2O_3 while these coordination numbers were close on CeO_2 support indicating a uniform distribution of Pd and Cu atoms. The CO shift activity was not simply correlated to the Cu-Cu bond distance or particle size, but the high activity of Pd-Cu/CeO_2 was attributed to surface Pd interacting with Cu on CeO_2 surface.

1. Introduction

Water gas shift (WGS) is one of the key steps in fuel processing for H_2 production for low-temperature fuel cell applications [1,2]. Cu-based catalysts have traditionally been employed for this reaction [3]. In the case of a Cu-Zn-Al oxide catalyst, a linear relationship was obtained between copper surface area and activity, but the linearity is not valid when the preparation method differs, meaning that the WGS is structure-sensitive [4]. Zinc and aluminum oxides are used as the support of catalyst where zinc addition increases the specific rate (activity per Cu surface area) through decrease of heat of CO adsorption [5] and increases dispersion of Cu while aluminum addition only disperses the Cu phase [6]. Although numerous efforts have been made for increasing activity and stability, the Cu-based catalysts have drawbacks of easy sintering and pyrophoricity [1].

CeO_2-supported Cu catalyst is one of the non-pyrophoric alternatives. While the surface of Cu/Al_2O_3 is saturated with a copper surface phase, fine CuO crystallites are formed on Cu/CeO_2/Al_2O_3 catalyst due to an interaction between the CeO_2 and copper phase [7]. Thus, the reaction pathway should be different. Copper is immiscible to CeO_2 lattice and enrichment of copper on the surface was identified by XPS [8]. Proposed active sites includes Cu^{1+} species that originates from interaction of copper clusters with oxygen species on ceria surface [9], and an isolated copper oxo species formed on CeO_2-containig supports [10].

In the effort to improve WGS activity at low temperature, our group has developed a method called oxygen-enhanced water gas shift (OWGS) in which a small amount of oxygen is added to a WGS feed [11]. Since catalyst should stand the oxidative condition, a new formulation, CeO_2-supported Pd-Cu and Pt-Cu catalysts, were developed. We have found that with these catalysts CO shift is significantly promoted by O_2 addition to the feed without deactivation [12]. Through kinetic analysis, we found that CO order is low on monometallic noble metal (Pd or Pt) due to high CO coverage on the active surface while CO order is high on Cu and it is moderate on Pd-Cu and Pt-Cu bimetallics. H_2O order showed an opposite trend to the CO order, which suggested that the reaction proceeds through the association of chemisorbed reactants [13]. By adding oxygen into the feed, only the CO order increased, which suggested that oxygen removes the chemisorbed CO to free up the sites for H_2O chemisorption and to balance these surface reactants. The oxygen addition did not promote CO shift on Al_2O_3-supported catalyst and low-surface-area CeO_2-supported catalyst (<2 m^2/g)

* Corresponding author.
** Corresponding author. Current address: Department of Applied Chemistry, Kobe City College of Technology, 8-3 Gakuen-higashimachi, Nishi-ku, Kobe, Hyogo 651-2194, Japan.
E-mail addresses: jkugai@kobe-kosen.ac.jp (J. Kugai), csong@psu.edu (C. Song).

http://dx.doi.org/10.1016/j.apcata.2016.09.010
0926-860X/

while over 90 m^2/g of surface area the turnover rate leveled off for CeO_2-supported catalysts [14]. However, the structural variation of Pd-Cu on different supports and its impacts on catalytic performance were not yet clear. In the present study, X-ray absorption fine structure of Pd-Cu bimetallic catalysts was investigated to find the factor to control the catalytic activity. We have also investigated the Pd-Cu structure in an in-situ CO shift atmosphere.

2. Experimental

The Pd-Cu bimetallic catalysts were prepared by incipient wetness co-impregnation using a mixed acetone solution of Pd (II) acetate and Cu (II) nitrate hemipentahydrate on ceria or alumina supports [14]. Three ceria supports, commercial HSA15 from Rhodia Co. (155 m^2/g of specific surface area, denoted as CeO_2(R)), another commercial CeO_2 from Rhodia (>200 m^2/g, denoted as CeO_2(H)), CeO_2 prepared by calcination of cerium (III) nitrate at 600 °C for 2 h (74 m^2/g, denoted as CeO_2(N)), and commercial alumina Puralox TH100/150 from Sasol (150 m^2/g, denoted as Al_2O_3) were used. All the samples were calcined at 450 °C for 5 h after co-impregnation of the precursors. The nominal metal loadings were approximately 2 wt.% for Pd and 5 wt.% or 10 wt.% for Cu. The catalyst composition is designated as Pd(2)Cu(5)/CeO_2(R), for instance, where inside the parenthesis following metal species is the metal loading in weight percent. The actual Cu/Pd atomic ratio in Pd(2)Cu(5)/CeO_2(R) was determined to be 4.18 using Inductively Coupled Plasma Atomic Emission Spectroscopy, which is close to the nominal value. For comparison, monometallic Cu catalyst was also prepared by impregnating aqueous solution of Cu(II) nitrate hemipentahydrate on CeO_2(R) support and monometallic Pd was prepared by impregnating acetone solution of Pd(II) acetate on CeO_2(R).

X-ray absorption measurements were conducted on the bending magnet beam line (10BM) of the Materials Research Collaborative Access Team (MRCAT) at the Advanced Photon Source, Argonne National Laboratory. The detailed method is described elsewhere [11]. The measurements were conducted in-situ with reduction atmosphere in transmission mode using a continuous-flow EXAFS reactor cell (18 in. long, 0.75 in diam.). The catalysts were reduced in 4% H_2/He at 260 °C for 30 min followed by purging with He at the same temperature for 30 min to desorb chemisorbed hydrogen and decompose Pd-H, followed by cooling to room temperature in He atmosphere. Then the Pd *K*-edge (24.350 keV) or Cu *K*-edge (8.979 keV) spectra were obtained. Spectra were also collected at 260 °C in He, 260 °C in H_2, and 260 °C in a model water gas shift feed (1%CO, 3%H_2O balanced by He). Spectra of Pd foil and Cu foil were acquired simultaneously with those of Pd-Cu/CeO_2 samples for energy calibration. Experimental phase and amplitude functions were prepared from Pd and Cu foil. Theoretical phase and amplitude functions for Pd-Cu and Cu-Pd were prepared using FEFF 8 and calibrated to Pd and Cu foils to determine the appropriate S_0, the Debye-Waller factor, and off-set in R.

The methods for catalytic test are described elsewhere [14]. About 0.1 g of the catalyst (sieved into 0.25–0.50 mm in diameter) was packed in a quartz fixed-bed down-flow reactor with 4 mm inner diameter (aspect ratio = ~1.5). The feed gas composition was 9.7% CO/22.8% H_2O/6.3% CO_2/37.9% H_2/6.9% air (1.4% O_2)/argon balance. For measuring WGS activity, the air was simply switched to nitrogen with the same flow rate. The space velocity was around 64,400 h^{-1} (dry, excluding air and argon). Prior to the catalytic reaction, catalyst was reduced in situ in 7.5% H_2/N_2 flow at 260 °C for 1 h.

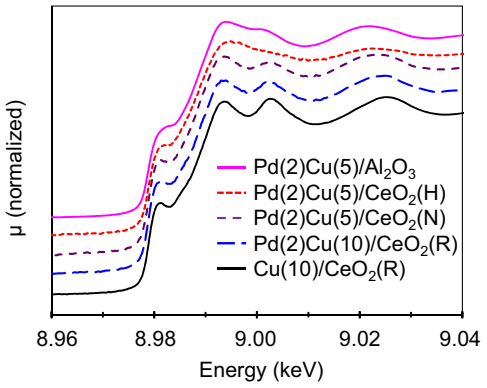

Fig. 1. Cu *K*-edge XANES of the catalysts measured at room temperature in helium after hydrogen reduction at 260 °C.
From the top, Pd(2)Cu(5)/Al_2O_3; Pd(2)Cu(5)/CeO_2(H); Pd(2)Cu(5)/CeO_2(N); Pd(2)Cu(10)/CeO_2(R); Cu(10)/CeO_2(R).

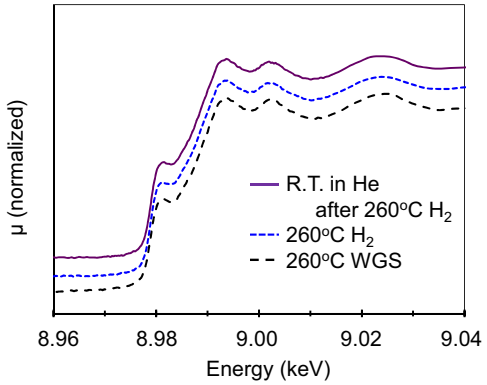

Fig. 2. Cu *K*-edge XANES of Pd(2)Cu(10)/CeO_2(R) catalysts measured in various conditions.
From the top, at room temperature in helium after hydrogen reduction at 260 °C; in hydrogen at 260 °C; in a WGS stream at 260 °C.

3. Results and discussion

3.1. Cu K-edge spectra

Fig. 1 shows Cu *K*-edge XANES spectra of Pd-Cu catalysts with various CeO_2 and Al_2O_3 supports in comparison with that of Cu(10)/CeO_2(R) catalyst. All the spectra were typical of metallic Cu. The edge energy and very similar shape of the XANES region for Pd(2)Cu(5)/CeO_2(N), Pd(2)Cu(10)/CeO_2(R), and Cu(10)/CeO_2(R) shows that the oxidation state and electronic structure of Cu is not much influenced by Pd addition. The slight shifts of the maximums of oscillation at around 9003 eV and 9020 eV towards lower energy by Pd addition could be an indication of a shorter first neighbor distance. The Pd addition to Cu leads to hybridation changes and charge transfer between Cu and Pd resulting in the small net charge transfer from Cu to Pd [15]. The white line in the XANES of Pd-Cu supported on CeO_2(H) and Al_2O_3 was slightly larger due to the presence of a small amount of oxidized Cu. A linear combination fit of the spectra to a combination of reference spectra (Cu^0, Cu^{1+} and Cu^{2+}) showed decrease of Cu^0 and increase of Cu^{1+} oxide. Fig. 2 compares the XANES spectra of Pd(2)Cu(10)/CeO_2(R) catalyst collected after various treatment conditions: in helium atmosphere at room temperature after reduction, in H_2 at 260 °C, and in a WGS stream at 260 °C. The XANES were basically identical suggesting little structural change occurs by heating or changing the atmosphere to the WGS stream after catalyst was reduced.

Table 1
Fitting parameters of Cu *K*-edge EXAFS spectra.

Sample	Condition	Scatter	N	R(Å)	DWF($\times 10^3$)	E_o(eV)	Particle size (Å)
Cu(10)/CeO_2(R)	He R.T.	Cu-Cu	11.0	2.55	1.0	0.9	75
Pd(2)Cu(5)/Al_2O_3	He R.T.	Cu-Cu	5.5	2.48	4.0	−7.6	14
	H_2 260 °C	Cu-Cu	5.5	2.46	8.0	−8.9	
	WGS 260 °C	Cu-Cu	5.5	2.47	8.0	−8.8	
Pd(2)Cu(5)/CeO_2(N)	He R.T.	Cu-Cu	7.3	2.50	3.0	−4.3	24
	H_2 260 °C	Cu-Cu	7.7	2.49	8.0	−5.5	
	WGS 260 °C	Cu-Cu	7.6	2.48	8.0	−6.7	
Pd(2)Cu(5)/CeO_2(H)	He R.T.	Cu-Cu	4.9	2.46	5.0	−8.2	12
Pd(2)Cu(10)/CeO_2(R)	He R.T.	Cu-Cu	9.0	2.53	2.0	−1.5	41

Fitting was conducted with k range of 2.8–10.8 $Å^{-1}$ and R range of 1–3 Å.

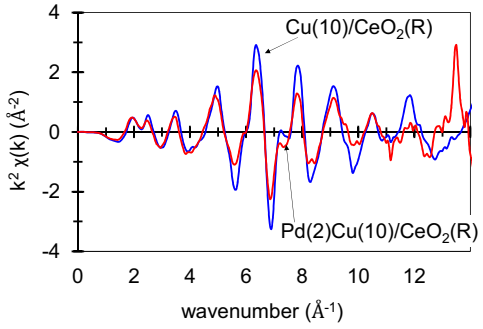

Fig. 3. Cu *K*-edge EXAFS oscillations in k space (k^2-weighting) of Cu(10)/CeO_2(R) and Pd(2)Cu(10)/CeO_2(R) catalysts.
Blue: Cu(10)/CeO_2(R); Red: Pd(2)Cu(10)/CeO_2(R) measured at room temperature in helium after hydrogen reduction at 260 °C. (For interpretation of the references to color in this figure legend, the reader is referred to the web version of this article.)

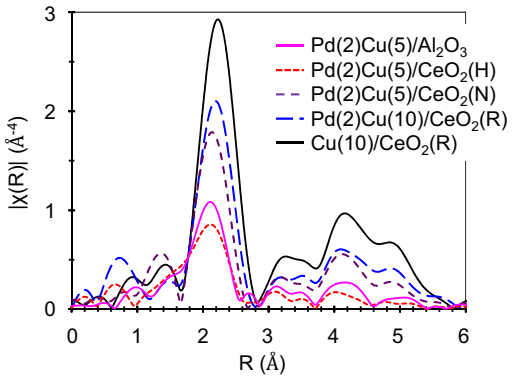

Fig. 4. Fourier transform of Cu *K*-edge EXAFS of the catalysts measured at room temperature in helium after hydrogen reduction at 260 °C.
k^2: Δk = 2.8–10.8; Pink: Pd(2)Cu(5)/Al_2O_3; dashed red: Pd(2)Cu(5)/CeO_2(H); dashed purple: Pd(2)Cu(5)/CeO_2(N); dashed blue: Pd(2)Cu(10)/CeO_2(R); black: Cu(10)/CeO_2(R). (For interpretation of the references to color in this figure legend, the reader is referred to the web version of this article.)

Fig. 3 shows typical Cu *K*-edge EXAFS oscillations in k space for monometallic Cu and bimetallic Pd-Cu catalysts and Fig. 4 shows the Fourier transform (FT) of various catalysts. For all the samples, the spectrum had a strong scattering at around 2.5 Å (phase corrected) which represents Cu neighbor. No Pd was apparent from the FT of Cu *K*-edge spectra likely due to the high Cu:Pd ratio. Peak intensity reflects the coordination number and therefore particle size. The peak intensity decreased significantly by Pd addition (Compare the FTs of Pd(2)Cu(10)/CeO_2(R) and Cu(10)/CeO_2(R)). The low-Cu samples containing 5 wt.% of Cu showed lower peak intensity than the samples containing 10 wt.% of Cu since the crystallites are smaller with low Cu content, as expected [16]. The Pd-Cu on CeO_2(H) and Al_2O_3 showed further lower peak intensity, meaning that their particle sizes are very small. Small-size particles have fraction of oxidized Cu as evidenced in the XANES spectra shown in Fig. 1; however, the Cu-O scattering was too small to be fit in the EXAFS in Fig. 4. One of the reasons for the formation of such small particles could be high specific surface area of these supports, over 200 m^2/g for CeO_2(H) and 150 m^2/g for Al_2O_3. However, support surface area is not a sole factor since Pd-Cu on CeO_2(R) has larger particles (~40 Å, see Table 1) regardless of the high specific surface area of CeO_2(R) (155 m^2/g). Other conceivable factor is the structure of support surface. In literature, it was reported that the coordination environment of Cu^{2+} ions depends on the exposed crystal plane of CeO_2 surfaces, a five-coordinated CuO on the (111) and (110) planes and an eight-coordinated CuO on the (100) plane, which results in the differences in the interactions of the components in the CuO/CeO_2 catalysts [17]. In a liquid-phase Pt/CeO_2 synthesis, the Pt size was significantly decreased by dehydrating CeO_2 through simply calcining the support at 600 °C [18]. It is also plausible that morphology of the support affects the Pd-Cu structure in the impregnation process. The structure of support surface, such as exposed crystal planes, hydrophobicity, and support morphology, could affect the strength of anchoring metal species on support surface in the reduction process.

Table 1 summarizes the fitting results of Cu *K*-edge spectra of supported Pd-Cu with various metal compositions and supports measured in various gas streams. For all catalysts containing both Pd and Cu, there was no indication of Pd neighbors in the fittings of EXAFS spectra even though the Pd *K*-edge analysis implies that Pd-Cu bonds exist (in a number of about 2.4 around each Cu for Pd(2)Cu(5)/Al_2O_3, given that Pd is surrounded by 9.8 Cu atoms and that the Pd/Cu atomic ratio is 0.24, see Table 2) and there is enough room for identifying them separately in view of the k range and R range used. This is likely due to the low Pd/Cu fraction in the catalyst and to similar bond distances for Cu-Pd and Cu-Cu which makes difficult to separate these oscillations. Though Cu *K*-edge EXAFS analysis did not give any indication of Pd neighbors, it gave rough number of neighbors around Cu. The fit of the Cu EXAFS shows that Cu-Cu bond distance of Pd-Cu catalyst is much shorter than that of monometallic Cu catalyst suggesting an electronic perturbation in these catalysts. The Pd-Cu bond distance is also short, close to or even shorter than Cu-Cu bond distance of pure copper, which will be shown later in the results of Pd *K*-edge spectra.

In an atomic-scale STM imaging combined with topography of tunneling conductance (dI/dV) for Pd-Cu alloy on Cu(111) surface, it was found that Pd atoms can substitute into Cu surface with little geometric changes [19]. The dI/dV topography showed Pd atoms dispersed in a Cu lattice are almost electronically identical to their host Cu atoms. In addition, Pd-Cu bonds are stronger than Pd-Pd or Cu-Cu bonds which drives Pd to be dispersed in Cu lattice. If Pd is readily dissolved and randomly distributed in the Cu NP's, the Cu

Table 2
Fitting parameters of Pd *K*-edge EXAFS spectra.

Sample	Condition	Scatter	N	R(Å)	DWF($\times 10^3$)	E_o(eV)	Particle size (Å)
Pd(4)/SBA-15	H_2 400 °C	Pd-Pd	8.1	2.73	1.0	−0.2	30
Pd(2)/CeO_2	He RT	Pd-Pd	5.5	2.71	4.0	−1.3	13
	WGS 260 °C	Pd-Pd	5.8	2.72	5.0	−0.5	
	WGS 350 °C	Pd-Pd	6.0	2.71	6.0	−0.4	
Pd(2)Cu(5)/Al_2O_3	He RT	Pd-Cu	9.8	2.56	2.0	−0.1	
	H_2 260 °C	Pd-Cu	9.6	2.54	6.5	−1.6	
	WGS 260 °C	Pd-Cu	9.8	2.54	6.5	−1.7	
	WGS 350 °C	Pd-Cu	9.8	2.53	8.0	−1.8	
Pd(2)Cu(5)/CeO_2(H)	He RT	Pd-Cu	5.4	2.53	4.0	−1.9	
Pd(2)Cu(5)/CeO_2(N)	He RT	Pd-Cu	7.8	2.56	3.0	1.4	
Pd(2)Cu(5)/CeO_2(R)	He RT	Pd-Cu	8.4	2.55	3.0	0.2	
	H_2 260 °C	Pd-Cu	8.4	2.53	7.0	−1.6	
	WGS 260 °C	Pd-Cu	8.5	2.55	7.0	−1.0	
	WGS 350 °C	Pd-Cu	8.5	2.54	7.5	−0.5	
Pd(2)Cu(10)/CeO_2(R)	He RT	Pd-Cu	9.8	2.56	3.0	1.3	
	H_2 260 °C	Pd-Cu	9.6	2.54	7.0	0.6	
	WGS 260 °C	Pd-Cu	10.3	2.54	7.0	-1.0	
	WGS 350 °C	Pd-Cu	10.3	2.54	7.5	-0.1	

Fitting was conducted with k range of 2.6–12.3 $Å^{-1}$ and R range of 1–3 Å.

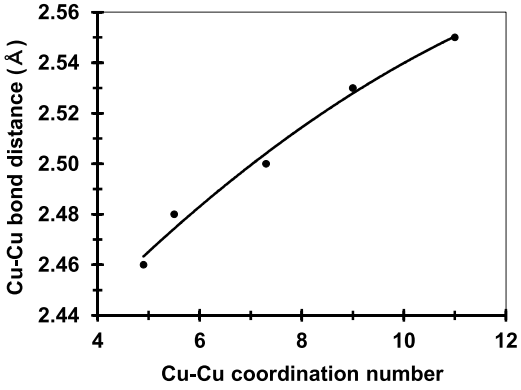

Fig. 5. Correlation between Cu-Cu coordination number and Cu-Cu bond distance in Pd-Cu catalysts.
The error range of bond length was about 0.02 Å in the fitting.

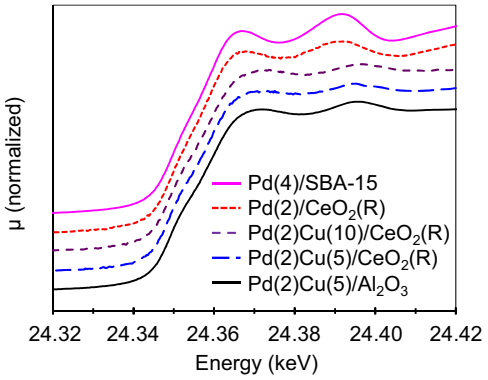

Fig. 6. Pd *K*-edge XANES of the catalysts measured at room temperature in helium after hydrogen reduction at 260 °C.
From the top, Pd(4)/SBA-15; Pd(2)/CeO_2(R); Pd(2)Cu(10)/CeO_2(R); Pd(2)Cu(5)/CeO_2(R); Pd(2)Cu(5)/Al_2O_3.

EXAFS would be expected to be dominated by the high fraction of Cu-Cu scattering.

Fig. 5 shows a relationship between Cu-Cu bond distance and Cu-Cu coordination number. The latter reflects particle size. The Cu-Cu bond distance decreased as the Cu-Cu coordination number decreased. When the coordination number was 11 for the monometallic Cu(10)/CeO_2 case, which corresponds to 75 Å of particle size, the bond distance was 2.55 Å, which is typical of the Cu-Cu distance of bulk copper. By adding Pd to Cu, the bond distance became even shorter than that of bulk copper. For the Pd(2)Cu(5)/CeO_2(N) sample, the coordination number was 7.3, which corresponds to 24 Å of particle size, the bond distance was 2.50 Å, which is clearly shorter than that of bulk copper. The lattice shrinkage becomes more remarkable when the size was smaller (R_{Cu-Cu} = 2.46 Å for the Pd(2)Cu(5)/CeO_2(H) sample), indicating that there is a strong electronic perturbation on Cu through interactions with Pd.

In EXAFS studies of supported Pd-Cu, bond lengths are not so shortened as that observed in the present study. Molenbroek et al. reported that Cu-Cu bond length is little influenced by a particle-size reduction of Pd-Cu on Al_2O_3 support although they also commented that the anharmonic vibrations cause underestimation of the coordination number for small particles [20]. Batista et al. investigated effect of metal loadings and reported no big impact on the bond distance in Pd-Cu/Al_2O_3 [21]. The Pd-Cu distance was roughly the arithmetic mean of distances of two monometallic systems. Fernandez-Garcia et al. showed that bond distance around a Cu center increases by c.a. 10% by alloying and that around a Pd center decreases by c.a. 2% by alloying [22]. Li et al. detected a slight lattice compression of Cu in their Cu@Pd core-shell nanowire by the XRD pattern [23]. They suggested a strain of the embracement of Pd layer as the reason, but no further detail was pursued. Compared to these reports, our Pd-Cu system exhibited a marked shrinkage of Cu owing to the very small particle size (<ca. 4 nm), which was realized by the preparation condition using palladium acetate as a metal source.

3.2. Pd K-edge spectra

Fig. 6 shows Pd *K*-edge XANES spectra of monometallic Pd and bimetallic Pd-Cu on various supports. The spectra of monometallic Pd were typical of bulk Pd while those of Pd-Cu samples were clearly different indicating formation of an alloy. The decrease in white line intensity indicates an increase of charge on the unoccupied orbitals of Pd. Many XPS studies show that there is electronic rearrangement induced by intermetallic bond, i.e. binding energy of Pd shifts to higher energy by Cu addition and that of Cu shifts to lower energy by Pd addition [24–27]. Some reports concluded that the charge moves from Pd to Cu based on XPS measurements while the others accounted the experimental results for hybridation and polarization of orbitals. Since the work function of Pd is ca. 0.5 eV higher than that of Cu, the latter is more probable. According to the theoretical study by Fernandez-Garcia et al., the charge in

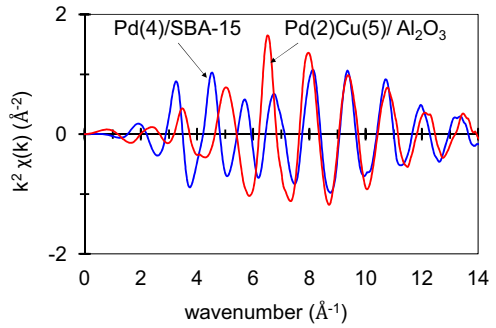

Fig. 7. Pd *K*-edge EXAFS oscillations in k space (k^2-weighting) of Pd(4)/SBA-15 and $Pd(2)Cu(5)/Al_2O_3$ catalysts.
Blue: Pd(4)/SBA-15 measured at room temperature in helium after hydrogen reduction at 400 °C; Red: $Pd(2)Cu(5)/Al_2O_3$ measured at room temperature in helium after hydrogen reduction at 260 °C. (For interpretation of the references to color in this figure legend, the reader is referred to the web version of this article.)

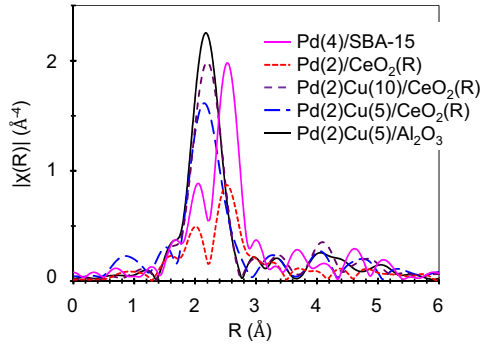

Fig. 8. Fourier transform of Pd *K*-edge EXAFS of the catalysts treated in hydrogen at 260 °C and cooled to room temperature in helium.
k^2: Δk = 2.6–12.3; Pink: Pd(4)/SBA-15; dashed red: $Pd(2)/CeO_2(R)$; dashed purple: $Pd(2)Cu(10)/CeO_2(R)$; dashed blue: $Pd(2)Cu(5)/CeO_2(R)$; black: $Pd(2)Cu(5)/Al_2O_3$. (For interpretation of the references to color in this figure legend, the reader is referred to the web version of this article.)

the Pd 4d and Cu 4sp subbands are decreased by polarization and charge transfer, respectively, and charge in the Pd 5sp subbands is increased by the Pd-Cu bond formation [15].

The spectra of monometallic Pd supported on CeO_2 or SBA-15 was very close to the Pd foil except that the amplitude of the XANES region for these samples was smaller than that of Pd foil (not shown in the figure). The smaller amplitude of the oscillation for $Pd(2)/CeO_2(R)$ compared to Pd(4)/SBA-15 would be due to the lower coordination number, which probably comes from low Cu loading and thus smaller particle size in the former. Among Pd-Cu samples, the XANES spectra were all similar regardless of Cu content. Highly dispersed Pd in Cu would make a similar environment. Also, the XANES spectra taken in helium at room temperature after H_2 reduction, in H_2 at 260 °C, and in WGS stream at 260 °C and 350 °C were identical though the spectra were not presented in the figure. Again, there was no effect of the atmosphere and temperature conditions on the local structure of Pd-Cu.

In Fig. 7, typical Pd *K*-edge EXAFS oscillations in k space for monometallic Pd and bimetallic Pd-Cu catalysts were presented and Fourier transforms of various catalysts were shown in Fig. 8. Two peaks at 2.5 Å and 2 Å (phase not corrected) in Fig. 8 are typical of monometallic Pd crystal. Smaller peaks for $Pd(2)/CeO_2(R)$ than Pd(4)/SBA15 is ascribed to lower Pd content and thus smaller particle size. The small peaks at R = 3.7, 4.6, and 5.1 Å seen in the

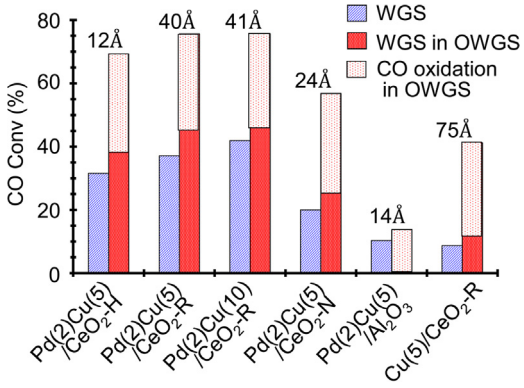

Fig. 9. WGS and OWGS activities of Pd-Cu catalysts on various supports.
Feed: 9.7% CO/22.8% H_2O/6.3% CO_2/37.9% H_2/6.9% N_2 (for WGS) or air (for OWGS) balanced by argon. Temperature: 260 °C. GHSV: 64,400 h^{-1} (dry).

FT of EXAFS spectra of Pd(4)/SBA-15 are coherent with the larger Pd particle size obtained for this catalyst since they coincide with the peaks in bulk Pd [28]. The Pd-Cu samples had a single peak at shorter distance indicating that the neighbor of Pd is mainly Cu. The fitting parameters were given in Table 2. In all the Pd-Cu catalysts, only Cu neighbors were visible, i.e. metallic Pd is surrounded by Cu atoms. The Pd-Pd bond distance in monometallic Pd was 2.72 Å, which is slightly shorter than that of Pd foil, 2.75 Å. The Pd-Cu bond distance in Pd-Cu catalysts was 2.55 Å, which is about 0.10 Å shorter than the sum of the atomic radii, (2.75 + 2.55)/2, or 2.65 Å, and close to that of Cu foil. The geometry of Pd neighbor seems very similar to the monometallic Cu [19].

The Al_2O_3-supported catalyst showed much lower coordination number for Pd-Cu obtained from Pd *K*-edge spectra than that for Cu-Cu obtained from Cu *K*-edge spectra while CeO_2-supported samples showed similar values. This means that the elemental distribution in the nanoparticles differs on Al_2O_3 and CeO_2 supports. On the former, Pd is primarily at the interior of the nanoparticles and with a Cu-rich surface, i.e., a Pd core-Cu shell morphology, while on the latter Pd and Cu are randomly distributed. It is known that Cu interacts with Al_2O_3 strongly to bring an enrichment of Cu on the surface of Pd-Cu particles when they are supported on Al_2O_3 support [21,29]. The surface enrichment is due partly to the lower surface free energy of Cu than Pd [30,31]. This also occurs on SiO_2 [20,31] and MCM-41[26], but lesser extent. For Pd-Cu/C prepared by a polyol method with citric acid stabilizer, Pd was more on the surface [32]. In this case, the presence of a strong adsorbate (citric acid in this case) would bring Pd to the surface [19]. Consistent with literature, Cu seems to interact strongly with Al_2O_3 in the present study while both Pd and Cu seem to interact with CeO_2. This is also inspired by our previous study of temperature-programmed reduction where Pd-Cu oxides were partly reduced in hydrogen below the room temperature on Al_2O_3 while Pd-Cu oxides were reduced simultaneously above room temperature on CeO_2 support [14]. The higher was the surface area of CeO_2, the less reducible was the metal species. The weaker interaction of Pd and Al_2O_3 could lead Pd to nucleate the metallic nanoparticles during the calcination in the air or in an early stage of the hydrogen reduction. On the other hand, the strong interaction of both Pd and Cu with CeO_2 would lead to homogeneous distribution of the two components in the particles.

3.3. Catalytic activities and Pd-Cu structure

The activity data for WGS and OWGS were presented in Fig. 9. The "WGS in OWGS" is the percentage equivalent to the net H_2 production and "CO oxidation in OWGS" is the difference of total

CO conversion and "WGS in OWGS". O_2 addition increased CO conversion significantly and net H_2 production to certain extent. Considering that Pd-containing catalysts show severe H_2 combustion (low selectivity for CO oxidation) with O_2 addition [33], promotion of CO shift would be significant on CeO_2-suported catalysts. On Al_2O_3-supported Pd-Cu, there was no WGS (H_2 production) in OWGS while there was a measurable WGS rate in the absence of O_2, which would be attributed to both lack of selectivity for CO oxidation and poor activity for CO shift. This difference is likely caused by the differences in Pd-Cu surface structure and metal-support interaction. Since Pd is distributed more in the interior of nanoparticles on Al_2O_3 support, the surface would have Cu character which less chemisorbs CO. In terms of the metal-support interaction, the activation of H_2O would be weak on Pd-Cu with Al_2O_3 support. Our previous kinetic study, in which the reaction order in CO drastically increased by O_2 addition to a WGS feed on CeO_2-supported Pd-Cu, but not on Al_2O_3-supported Pd-Cu, led to the conclusion that O_2 addition removes a part of CO to free up the sites for H_2O chemisorption and effectively to activate H_2O on CeO_2-supported Pd-Cu [14].

Although there is no data taken in a gas containing O_2 and thus XAS spectra in OWGS conditions could be different from those in WGS conditions, we think the structural change in the presence of O_2 is minor for two reasons. First, the local structure (XANES spectra) of copper in Pt-Cu/CeO_2 was almost identical for H_2 stream and PROX stream (10%CO, 5%O_2, 10%H_2, and N_2 balance) at 100 °C according to literature [34]. Second, Haruta et al. observed only surface morphology change in Au nanoparticle supported on CeO_2 in various CO/air mixed atmospheres using in-situ TEM technique. When CO/air ratio was small, the edge site of Au particle became round, suggesting some surface rearrangement of atoms occurred [35]. Though Pd-Cu is more vulnerable to an oxidizing atmosphere than the Au/CeO_2 system, our OWGS condition is quite reducing (O_2 is present in excess H_2), thus the bulk structure of Pd-Cu would not change much by the addition of small amount of O_2 and change of nanoparticle structure would be rather superficial.

Among the CeO_2-supported Pd-Cu, the catalysts with high-surface-area CeO_2 support tends to give high catalytic activity, but it is not strictly true, e.g. Pd-Cu/CeO_2(R) is more active than Pd-Cu/CeO_2(H), meaning that CeO_2 surface area is not a sole factor controlling the reaction. Also, activity was irrelevant to the alloy particle size estimated from the Cu *K*-edge EXAFS, meaning that the peripheral length of alloy particles (metal-CeO_2 interfacial length) is not a direct factor either. The structure of metal-CeO_2 interface or the balance of electronic interactions among Pd, Cu, and CeO_2 could be of importance. The electronic interaction between two metal components on CeO_2 was different from those on other supports as evidenced by the less reducible property in our previous TPR study.

It should be noted that Pd(2)Cu(5)/CeO_2(R) outperformed Pd(2)Cu(5)/CeO_2(H) in the OWGS stream containing H_2 and CO_2 while these catalysts performed almost identically in an OWGS stream without H_2 and CO_2 [14]. One negative factor for high surface area CeO_2 would be a slow CO_2 desorption and easy accumulation of carbonate on the surface. Another negative factor could be the small Pd-Cu nanoparticle size. In methanol electrooxidation reaction, the size reduction of Pt catalyst below 5 nm drastically increases the number of unsaturated Pt atoms on the surface, which causes strong retention of intermediate CO [36,37] and oxygenated species like OH [38,39]. Similar negative effect is possible for the present Pd-Cu system. The metal-support interaction and/or interfacial structure could affect these chemisorption properties of intermediates and products. Further investigation is necessary for elucidating the quantitative contributions of the two factors.

4. Conclusions

Using the X-ray absorption technique, the local structures of Pd and Cu in Pd-Cu catalysts were investigated in comparison with monometallic catalysts. From Cu *K*-edge spectra, only Cu neighbors were recognized and Pd neighbor was invisible. The particle size estimated from the Cu-Cu coordination number was much smaller for Pd-Cu system than monometallic Cu. The Cu-Cu bond distance in the Pd-Cu system was much shorter than that of monometallic Cu, which was correlated to the small particle size. The Pd *K*-edge XANES looks like an alloy, but in the EXAFS spectra, only Cu neighbors were identified. Thus, Pd is atomically dispersed in the Cu lattice. The Fourier transform of Pd *K*-edge spectra showed that Pd is geometrically identical to Cu, i.e. the Pd-Cu bond distance is much shorter than that of monometallic Pd (2.75 Å) and is close to Cu-Cu bond distance of monometallic Cu (2.55 Å). Although such structural feature (small particle size and lattice shrinkage) of Pd-Cu is not a sole factor for the enhanced CO shift activity, the interactions among these two metal components and CeO_2 support were suggested to control the CO shift activity.

Acknowledgments

We wish to thank the U.S. Department of Energy, National Energy Technology Laboratory and US Office of Naval Research for partial support of this work on liquid fuel processing for fuel cells. Use of the Advanced Photon Source is supported by the U.S. Department of Energy, Office of Science, and Office of Basic Energy Sciences, under Contract DE-AC02-06CH11357. MRCAT operations are supported by the U.S. Department of Energy and the MRCAT member institutions. Savannah River National Laboratory is operated by Savannah River Nuclear Solutions. This document was prepared in conjunction with work accomplished under Contract No. DE-AC09-08SR22470 with the U.S. Department of Energy. We also thank Rhodia Co. for generously supplying CeO_2 support. Analysis of catalyst composition was conducted with help of the group of Prof. Takao Yamamoto at Osaka University.

References

[1] A.F. Ghenciu, Curr. Opin. Solid State Mater. Sci. 6 (2002) 389–399.
[2] C.S. Song, Catal. Today 77 (2002) 17–49.
[3] D.C. Grenoble, M.M. Estadt, D.F. Ollis, J. Catal. 67 (1981) 90–102.
[4] R.A. Hadden, P.J. Lambert, C. Ranson, Appl. Catal. A: Gen. 122 (1995) L1–L4.
[5] R.N. d'Alnoncourt, M. Kurtz, H. Wilmer, E. Loffler, V. Hagen, J.Y. Shen, M. Muhler, J. Catal. 220 (2003) 249–253.
[6] M. Saito, K. Murata, Catal. Surv. Asia 8 (2004) 285–294.
[7] P.K. Cheekatamarla, C.M. Finnerty, J. Power Sour. 160 (2006) 490–499.
[8] W. Liu, M. Flytzani-Stephanopoulos, J. Catal. 153 (1995) 317–332.
[9] X.Q. Wang, J.A. Rodriguez, J.C. Hanson, D. Gamarra, A. Martinez-Arias, M. Fernandez-Garcia, J. Phys. Chem. B 110 (2006) 428–434.
[10] P. Ratnasamy, D. Srinivas, C.V.V. Satyanarayana, P. Manikandan, R.S.S. Kumaran, M. Sachin, V.N. Shetti, J. Catal. 221 (2004) 455–465.
[11] E.B. Fox, S. Velu, M.H. Engelhard, Y.H. Chin, J.T. Miller, J. Kropf, C.S. Song, J. Catal. 260 (2008) 358–370.
[12] J. Kugai, J.T. Miller, N. Guo, C. Song, J. Catal. 277 (2011) 46–53.
[13] J. Kugai, E.B. Fox, C. Song, Appl. Catal. A: Gen. 497 (2015) 31–41.
[14] J. Kugai, E.B. Fox, C. Song, Appl. Catal. A: Gen. 456 (2013) 204–214.
[15] M. Fernández-García, J.C. Conesa, A. Clotet, J.M. Ricart, N. López, F. Illas, J. Phys. Chem. B 102 (1998) 141–147.
[16] K.A. Guy, H. Xu, J.C. Yang, C.J. Werth, J.R. Shapley, J. Phys. Chem. C 113 (2009) 8177–8185.
[17] L. Liu, Z. Yao, Y. Deng, F. Gao, B. Liu, L. Dong, ChemCatChem 3 (2011) 978–989.
[18] J. Kugai, T. Moriya, S. Seino, T. Nakagawa, Y. Ohkubo, H. Nitani, T. Akita, Y. Mizukoshi, T.A. Yamamoto, Chem. Eng. J. 223 (2013) 347–355.
[19] H.L. Tierney, A.E. Baber, E.C.H. Sykes, J. Phys. Chem. C 113 (2009) 7246–7250.
[20] A.M. Molenbroek, S. Haukka, B.S. Clausen, J. Phys. Chem. B 102 (1998) 10680–10689.
[21] J. Batista, A. Pintar, J.P. Gomilšek, A. Kodre, F. Bornette, Appl. Catal. A: Gen. 217 (2001) 55–68.
[22] M. Fernandez-Garcia, J.A. Anderson, G.L. Haller, J. Phys. Chem. 100 (1996) 16247–16254.
[23] S. Li, D. Cheng, X. Qiu, D. Cao, Electrochim. Acta 143 (2014) 44–48.

[24] B.L. Gustafson, P.S. Wehner, Appl. Surf. Sci. 52 (1991) 261–270.
[25] S.Z. Hu, L. Scudiero, S. Ha, Electrochem. Commun. 38 (2014) 107–109.
[26] P. Benito, M. Gregori, S. Andreoli, G. Fornasari, F. Ospitali, S. Millefanti, M.S. Avila, T.F. Garetto, S. Albonetti, Catal. Today 246 (2015) 108–115.
[27] S. Sitthisa, T. Pham, T. Prasomsri, T. Sooknoi, R.G. Mallinson, D.E. Resasco, J. Catal. 280 (2011) 17–27.
[28] K. Sasaki, H. Naohara, Y.M. Choi, Y. Cai, W.F. Chen, P. Liu, R.R. Adzic, Nat. Commun. 3 (2012) 1115.
[29] A.B. Hungria, A. Iglesias-Juez, A. Martinez-Arias, M. Fernandez-Garcia, J.A. Anderson, J.C. Conesa, J. Soria, J. Catal. 206 (2002) 281–294.
[30] A. Renouprez, K. Lebas, G. Bergeret, J. Mol. Catal. A: Chem. 120 (1997) 217–225.
[31] S. Lambert, B. Heinrichs, A. Brasseur, A. Rulmont, J.P. Pirard, Appl. Catal. A: Gen. 270 (2004) 201–208.
[32] L. Wang, J.J. Zhai, K. Jiang, J.Q. Wang, W.B. Cai, Int. J. Hydrogen Energy 40 (2015) 1726–1734.
[33] J. Kugai, J.T. Miller, N. Guo, C.S. Song, Appl. Catal. B: Environ. 105 (2011) 306–316.
[34] J. Kugai, T. Moriya, S. Seino, T. Nakagawa, Y. Ohkubo, H. Nitani, T.A. Yamamoto, Catal. Lett. (2013).
[35] T. Uchiyama, H. Yoshida, Y. Kuwauchi, S. Ichikawa, S. Shimada, M. Haruta, S. Takeda, Angew. Chem. Int. Ed. 50 (2011) 10157–10160.
[36] K. Kinoshita, J. Electrochem. Soc. 137 (1990) 845–848.
[37] J. Perez, E.R. Gonzalez, E.A. Ticianelli, Electrochim. Acta 44 (1998) 1329–1339.
[38] A. Gamez, D. Richard, P. Gallezot, F. Gloaguen, R. Faure, R. Durand, Electrochim. Acta 41 (1996) 307–314.
[39] Y. Takasu, N. Ohashi, X.G. Zhang, Y. Murakami, H. Minagawa, S. Sato, K. Yahikozawa, Electrochim. Acta 41 (1996) 2595–2600.